Pressure Affects the Structure and the Dynamics of the D-Galactose/D-Glucose-Binding Protein from *Escherichia coli* by Perturbing the C-Terminal Domain of the Protein†

Anna Marabotti,‡,§ Alessio Ausili,§,|| Maria Staiano,⊥ Andrea Scirè,|| Fabio Tanfani,|| Antonietta Parracino,⊥ Antonio Varriale,⊥ Mosè Rossi,⊥ and Sabato D'Auria*,⊥

Laboratorio di Bioinformatica, Istituto di Scienze dell'Alimentazione, CNR, Avellino, Italy, Istituto di Biochimica, Università Politecnica delle Marche, Ancona, Italy, and Istituto di Biochimica delle Proteine, CNR, Napoli, Italy

Received June 10, 2006; Revised Manuscript Received July 14, 2006

ABSTRACT: The effect of the pressure on the structure and stability of the D-galactose/D-glucose binding protein from *Escherichia coli* in the absence (GGBP) and in the presence (GGBP/Glc) of glucose was studied by Fourier transform infrared (FT-IR) spectroscopy and molecular dynamic (MD) simulations. FT-IR spectroscopy experiments showed that the protein β-structures are more resistant than α-helices structures to pressure value increases. In addition, the infrared data indicated that the binding of glucose stabilizes the protein structure against high pressure values, and the protein structure does not completely unfold up to pressure values close to 9000 bar. MD simulations allow a prediction of the most probable configuration of the protein, consistent with the increasing pressures on the two systems. The detailed analysis of the structures at molecular level confirms that, among secondary structures, α-helices are more sensitive than β-structures to the destabilizing effect of high pressure and that glucose is able to preserve the structure of the protein in the complex. Moreover, the evidence of the different resistance of the two domains of this protein to high pressure is investigated and explained at a molecular level, indicating the importance of aromatic amino acid in protein stabilization.

The study of the effect of high pressure on structure, function, and dynamics of proteins has gained increasing interest during last years. In fact, pressure stress is proving itself as an invaluable tool for the exploration of biological functions. Considerable advances in the utilization of high-pressure techniques in food science and technology (*1*) have been made, and there are some attempts to extend their use to medical and pharmaceutical fields (*2*). Moreover, one of the most intriguing goals of high-pressure studies is the characterization of folding and unfolding processes of proteins (*3*−*5*). In fact, pressure is generally considered as a potential denaturant of proteins, with the great advantage that it affects only the volume of the system, whereas temperature denaturation involves changes in both the volume and the thermal energy. Moreover, while denaturation by pressure is generally reversible, temperature denaturation often results in irreversible aggregation (*6*). Thus, it is extremely interesting to study the influence of pressure on protein structure and function. This information is of outstanding importance, especially when a protein is considered as a potential candidate for its use as a biosensor (*7*) since the application of nonthermal processes as an alternative or together with conventional preservation methods can enhance their global antimicrobial effect (*2*, *8*).

During past decades, a plethora of experimental approaches have been used to characterize structure−function relationships of a protein submitted to a high-pressure stress (*9*). Among all these approaches, Fourier transform infrared (FT-IR)[1] spectroscopy coupled with the application of a diamond anvil cell showed very exciting developments in this field, since it enables the investigation of the protein secondary structure even under extremely high pressure. Several examples of its usefulness are reviewed, especially concerning protein aggregation, amyloid formation, and the protein folding thermodynamics related to single structural features (*10*).

On the other hand, molecular dynamics (MD) simulations can assist the interpretation of experimental data, since they start from a physical mechanical model of molecules and reproduce in silico the possible changes in conformation induced by energy and/or volume perturbations. Conforma-

† This work was supported by the ASI project MoMa n. 1/014/06/0, by a grant from the Ministero degli Affari Esteri, Direzione Generale per la Promozione e la Cooperazione Culturale (SD, MS, MR), by CRdC-ATIBB POR UE-Campania Mis 3.13 activities (SD, MR), by a grant from Università Politecnica delle Marche (FT), and by the CNR Commessa Diagnostica avanzata ed alimentazione (SD).

* Corresponding author: Dr. Sabato D'Auria, Institute of Protein Biochemistry, Italian National Research Council, Via Pietro Castellino, 111, 80131 Naples, Italy. Phone: +39-0816132250. Fax: +39-0816132277. E-mail: s.dauria@ibp.cnr.it.

‡ Istituto di Scienze dell'Alimentazione, CNR.

§ A.M. and A.A. contributed equally to the work.

|| Università Politecnica delle Marche.

⊥ Istituto di Biochimica delle Proteine, CNR.

[1] Abbreviations: GGBP, D-galactose/D-glucose-binding protein in the absence of glucose; GGBP/Glc, GGBP in the presence of 10 mM glucose; FT-IR, Fourier transform infrared; amide I′, amide I band in ^2H_2O medium; $P_{1/2}$, pressure of protein melting; MD, molecular dynamics.

10.1021/bi061158k CCC: $33.50
Published on Web 09/09/2006

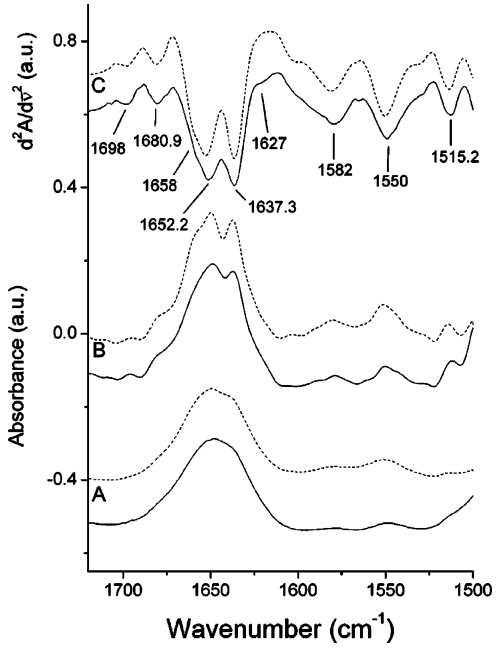

FIGURE 1: Absorbance (A), deconvolved (B), and second-derivative (C) spectra of GGBP and GGBP/Glc at p^{2}H 7.0. Continuous and dashed lines represent the spectra of GGBP and of GGBP/Glc, respectively. The spectra were obtained from samples introduced in a diamond anvil cell (Cryocell, Diacell Products, Leicester, U.K.) maintained at 20 °C and 1 bar.

tional states sampled by MD simulations at high pressure are not fully relaxed in the thermodynamic sense, but have undergone only elastic relaxation. Nonetheless, the study of these pre-denatured states has provided useful information about the response of native proteins to external pressure and, as a consequence, some clues about pressure-induced denaturation (*11*).

In our previous work (*12*), we applied steady-state and time-resolved fluorescence spectroscopy to investigate the effects of moderate pressure (up to 2000 bar) on the structure and function of D-galactose/D-glucose binding protein (GGBP) from *Escherichia coli*, the primary receptor for a high-affinity transport complex of the two sugars and for chemotaxis toward glucose and galactose (*13*). This protein can be a good candidate for its use as an implantable biosensor for glucose determination, e.g. to measure glucose concentration in the interstitial fluid of diabetic patients (*7*); as a consequence it is of interest to explore the effect of nonthermal methods, e.g. high pressure, used to sterilize devices before their utilization.

In the current work, we present a further characterization of the effect of high pressure on the structure of this protein by means of FT-IR spectroscopy and MD simulations. The results of infrared spectroscopy show the progressive loss in secondary structures and particularly highlight that β-structures are more resistant than α-helices to pressure stress. Moreover, it is clearly demonstrated that the presence of glucose is able to preserve the structure of the protein against denaturation.

MD simulations allow us to predict what are the molecular features mostly affected by the pressure influence not only in global terms but also singularly and the evolution of their perturbation at increasing pressures. This allows us to give

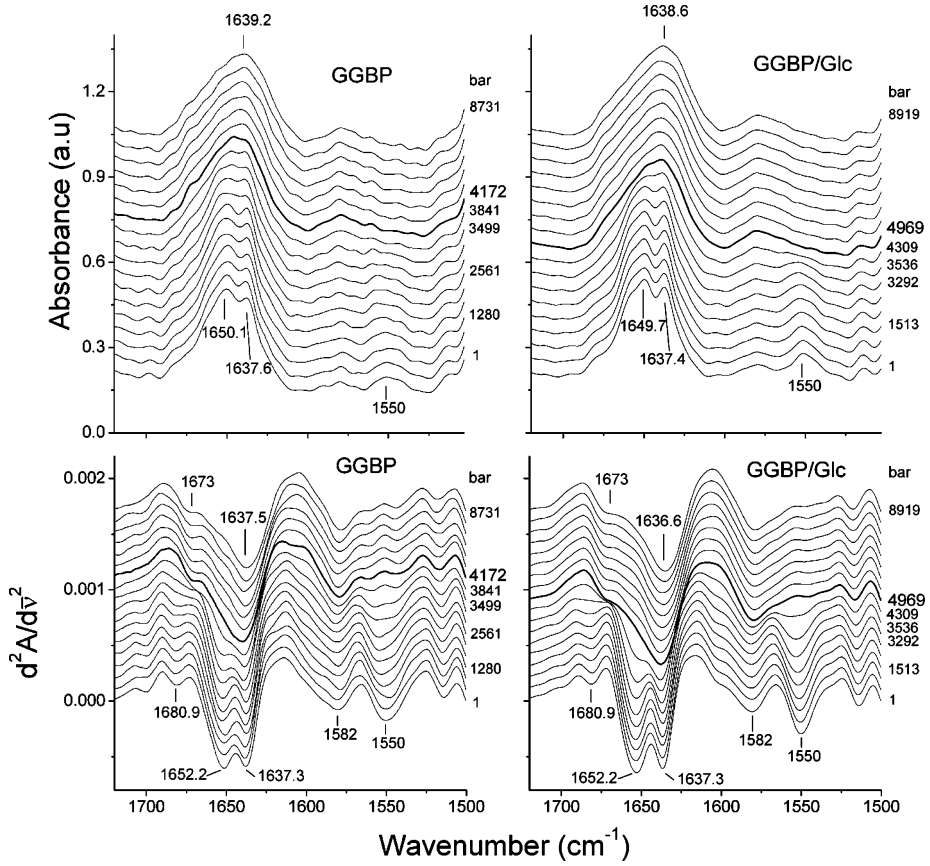

FIGURE 2: Deconvolved (top) and second-derivative (bottom) spectra of GGBP and of GGBP/Glc as a function of applied hydrostatic pressure. The spectra were obtained at 20 °C.

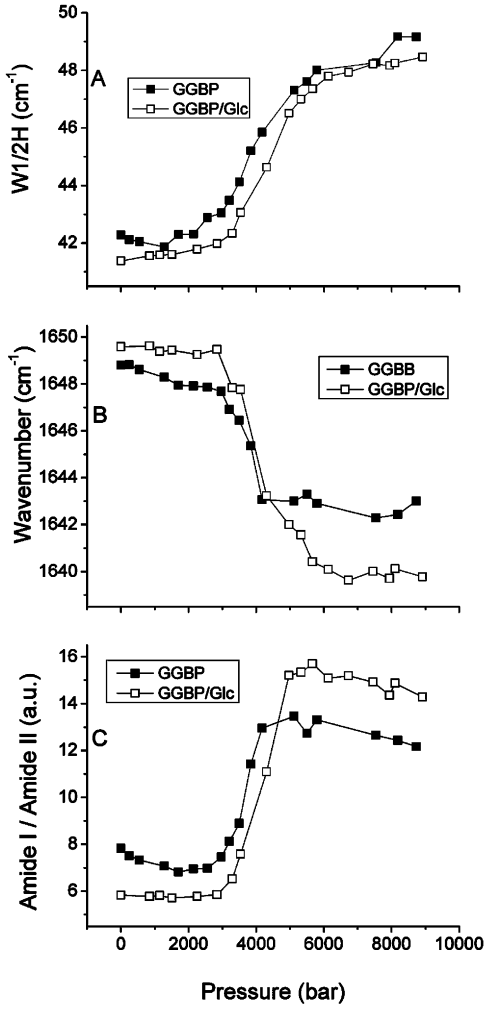

FIGURE 3: Pressure-dependent changes in absorbance spectra of GGBP and GGBP/Glc. Panels A, B, and C show the pressure-dependent changes in width and position of amide I′ band, and the pressure-dependent changes in amide I′/amide II intensity ratio, respectively. The width of the amide I′ band was calculated at $^1/_2$ of the amide I′ band intensity (W1/2H).

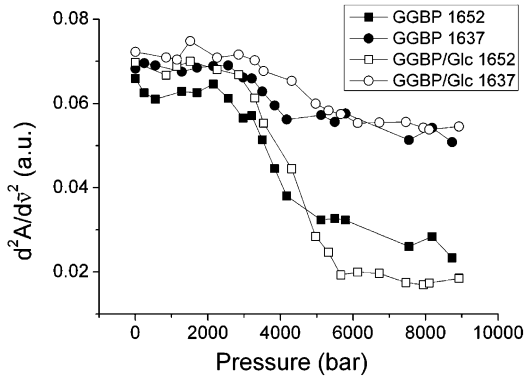

FIGURE 4: Pressure-dependent changes in the intensity of α-helix (1652 cm^{-1}) and β-sheet (1637 cm^{-1}) bands. The data were obtained from the second-derivative spectra (Figure 2). The reported data were multiplied by a factor of 100.

a "molecular portrait" of the protein that underwent the pressure perturbation and to interpret the spectroscopic data in full details. The detailed analysis of amino acid interactions in the structure is also able to explain the different sensitivity of the two protein domains to the negative influence of high external pressure.

Table 1: Midpoint Transitions ($P_{1/2}$) Derived from the Curves Obtained by Monitoring Different Parameters of Infrared Spectra as a Function of the Applied Hydrostatic Pressure

parameter[a]	$P_{1/2}$ in GGBP (bar)	$P_{1/2}$ in GGBP/Glc (bar)
$W_{1/2}$AI′ ↑	3890	4210
position AI′ ↓	3863	4189
AI′/AII ↑	3780	4160
α ↓	3750	4170
β ↓	3850	4250
AII ↓	3730	3805

[a] The symbols ↑ or ↓ indicate the pressure-dependent increase or decrease of the value of the corresponding parameter, respectively. $W_{1/2}$AI′: width of amide I′ band measured at $^1/_2$ of amide I′ band eight of absorbance spectra. Position AI′: position of amide I′ band in absorbance spectra. AI′/AII: amide I′/amide II intensity ratio in absorbance spectra. α: intensity of the α-helix band in the second-derivative spectra. β: intensity of the β-sheet band in the second-derivative spectra. AII: amide II intensity in absorbance spectra.

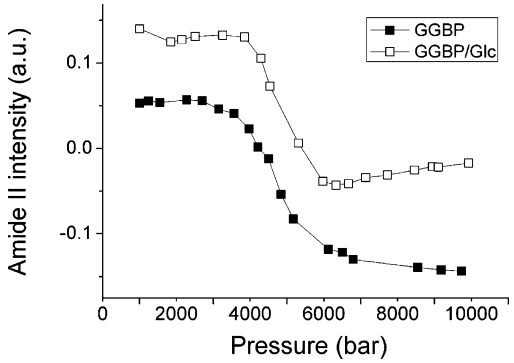

FIGURE 5: Pressure-dependent changes in intensity of the residual amide II band. The data were obtained from absorbance spectra.

MATERIALS AND METHODS

D-Glucose was purchased from Sigma. Deuterium oxide (99.9% ^2H_2O), ^2HCl, and NaO^2H were purchased from Aldrich. All other chemicals were commercial samples of the highest purity.

Protein Purification. D-Galactose/D-glucose binding protein from *E. coli* was prepared and purified according to previously reported procedures (*14*). Concentrated stock solutions of purified GGBP were dialyzed against 10 mM Tris/HCl, pH 7.0.

Protein Determination. The method of Bradford with bovine serum albumin as a standard was used for the determination of the protein concentration (*15*). A double beam Cary 1E spectrophotometer (Varian, Mulgrade, Victoria, Australia) was used for OD measurements.

Preparation of Samples for Infrared Measurements. Typically 2.0−2.5 mg of protein dissolved in the original buffer used for the purification were centrifuged in a 30K Centricon microconcentrator (Amicon) at 3000*g* and 4 °C and concentrated into a volume of approximately 40 μL. Then, 200 μL of buffer A (25 mM Hepes p^2H 7.0) or buffer B (25 mM Hepes, 10 mM glucose p^2H 7.0) were added and the sample concentrated again; the p^2H value corresponds to the pH-meter reading + 0.4 (*16*, *17*). This procedure was repeated several times in order to replace the original buffer with buffer A or buffer B. In the last washing the protein sample was concentrated to approximately 6% (w/v) and used for the infrared measurements.

Table 2: DSSP Analysis of the Average Structures Obtained by MD for GGBP and GGBP/Glc at Different Pressure Values[a]

	initial	avg external pressure (bar) on 0.2 ns MD run					
parameters	0	500	1000	2000	3000	4000	5000
			GGBP				
α-helices[b]	41.4	9.7	11.3	10.3	10.4	12.9	11.7
β-structures[c]	18.4	15.2	9.4	10.3	5.2	5.8	5.2
others[d]	25.6	45.0	41.4	42.8	44.3	42.1	42.1
random coil[e]	14.6	30.1	37.9	36.6	40.1	39.2	41.1
			GGBP/Glc				
α-helices[b]	41.4	32.4	27.2	23.3	21.3	18.0	19.0
β-structures[c]	19.1	18.1	19.1	18.8	16.4	13.4	14.4
others[d]	25.4	27.2	30.7	30.8	33.1	37.1	37.1
random coils[e]	14.1	22.3	23.6	25.1	29.2	31.5	29.5

[a] The results for pressures up to 2000 bar refer to data published in Marabotti et al. (*9*) and are reported here to aid the comparison. [b] Marked as "H" in DSSP output. [c] Marked as "E" in DSSP output. [d] Marked as "B", "G", "I", "S", and "T" in DSSP output. [e] Structures not classified in DSSP output.

Infrared Spectra. A proper amount of the concentrated protein sample and of dry $BaSO_4$ was placed in a 0.5 mm hole made in a 25 μm stainless steel gasket placed between two diamonds of a thermostatted diamond anvil cell (Cryocell) (Diacell Products, Leicester, U.K.). Pressure inside the anvil cell was generated by high-pressure nitrogen and controlled by a G-01 gas-membrane control box (Diacell Products, Leicester, U.K.). The hydrostatic pressure was measured by the shift of the sulfate-stretching band of $BaSO_4$ at 983 cm^{-1} as described (*18*). The temperature was maintained at 20 °C using an external bath circulator (HAAKE F6). Infrared spectra were recorded at 2 cm^{-1} resolution by means of a Nicolet Nexus FT-IR spectrometer equipped with a liquid-nitrogen-cooled mercury−cadmium−telluride (MCT) detector. At least 24 h before and during data acquisition, the spectrometer was continuously purged with dry air at a dew point of −70 °C. Typically, 256 scans were averaged for each spectrum obtained at a specific pressure. The protein samples prepared in buffer A or buffer B were analyzed in the 1−8731 bar range or in the 1−8919 bar pressure range, respectively. After each pressure increase the protein solution was allowed to equilibrate for 10 min before taking the infrared spectrum (*19*). Spectra were processed using the SPECTRUM software from Perkin-Elmer. Second-derivative spectra were calculated over a 19-data-point range (19 cm^{-1}), and the parameters of deconvolution were set with a γ value of 3.5 and a smoothing length of 75. The midpoint transition ($P_{1/2}$) in the pressure-induced denaturation curves was calculated as described (*20*).

Computational Analysis. The program Insight II (version 2000.1, 2000; Accelrys) was used throughout the calculations. The starting points for this series of simulations are the output files from the MD simulations at 2000 bar previously obtained for both GGBP alone and the GGBP/Glc complex (*12*). All conditions used in the previous investigations (*12*) were maintained in the present work. In particular, the CVFF force field was applied during calculations, and potentials and charges were set accordingly. We performed the MD run using the Verlet velocity algorithm, at time step of 1 fsec, with the NPT (constant temperature and constant pressure) ensemble. Pressure was set at 3000, 4000, and 5000 bar with the Parrinello−Rahman method in three subsequent simulations (the final conformation of each pressure was used as input for the following simulation at higher pressure). The settings for the periodic boundary conditions were also adopted as previously described (*12*), and the temperature was fixed at 298 K in all cases and controlled with the Berendsen's method of bath coupling. Each MD was run for 0.2 ns, taking results of the system during dynamics every 1 ps.

To analyze the different effects of the pressure on geometry and structural features of GGBP and GGBP/Glc, the conformations obtained for each pressure step were "averaged" in a unique structure with the aid of Insight II tools. The program DSSP (*21*) was then used to determine the relative position and percentage of secondary structure elements in these "average structures" obtained from the dynamics runs. The program NACCESS (*22*) was also used to calculate the solvent accessibility of the aromatic amino acids, using a probe atom of 1.40 Å rolling on the van der Waals surface of the protein models.

RESULTS AND DISCUSSION

Secondary Structure of GGBP and GGBP/Glc. The effect of glucose binding on the structure and thermal stability of *E. coli* GGBP was investigated previously by us (*23*−*25*). Here we report the effect of hydrostatic pressure on the structure of GGBP and of GGBP/Glc. The absorbance, deconvolved, and second-derivative infrared spectra of the protein in the absence and in the presence of glucose are shown in Figure 1. The resolution-enhanced spectra obtained at 1 bar show the bands observed in the previous studies (*24*, *25*). In particular, typical α-helix bands are displayed at 1658 and 1652.2 cm^{-1} (*26*); the former band was previously assigned to a population of α-helices with low exposure to the solvent (*23*). The 1698, 1637.3, and 1627 cm^{-1} bands are due to β-sheets (*26*, *27*) while the 1680.9 cm^{-1} absorption may be due to turns and/or β-sheets (*26*, *28*). Absorptions of tyrosine and of the ionized carboxyl group of aspartic acid are visible at 1515.2 and 1582.0 cm^{-1}, respectively (*29*−*31*). The small absorption at 1550 cm^{-1} represents the amide II (residual amide II band) that, in ^2H_2O medium, underwent a marked decrease in intensity proportional to the extent of exchange of amide hydrogens with deuterium ($^1H/^2H$) (*23*, *32*). The intensity of the residual amide II band gives a measure of the accessibility of the solvent (^2H_2O) to the protein: the higher the intensity, the lower the solvent accessibility. Hence, the residual amide II band shown in the spectra reported in Figure 1 indicates that ^2H_2O was not completely accessible to GGBP or GGBP/Glc, suggesting that part of the protein possesses a particu-

Scheme 1: Schematic Representation of the Changes in Secondary Structures (α-Helices and β-Sheets) of GGBP Subjected to Pressure Increases up to 5000 Bar[a]

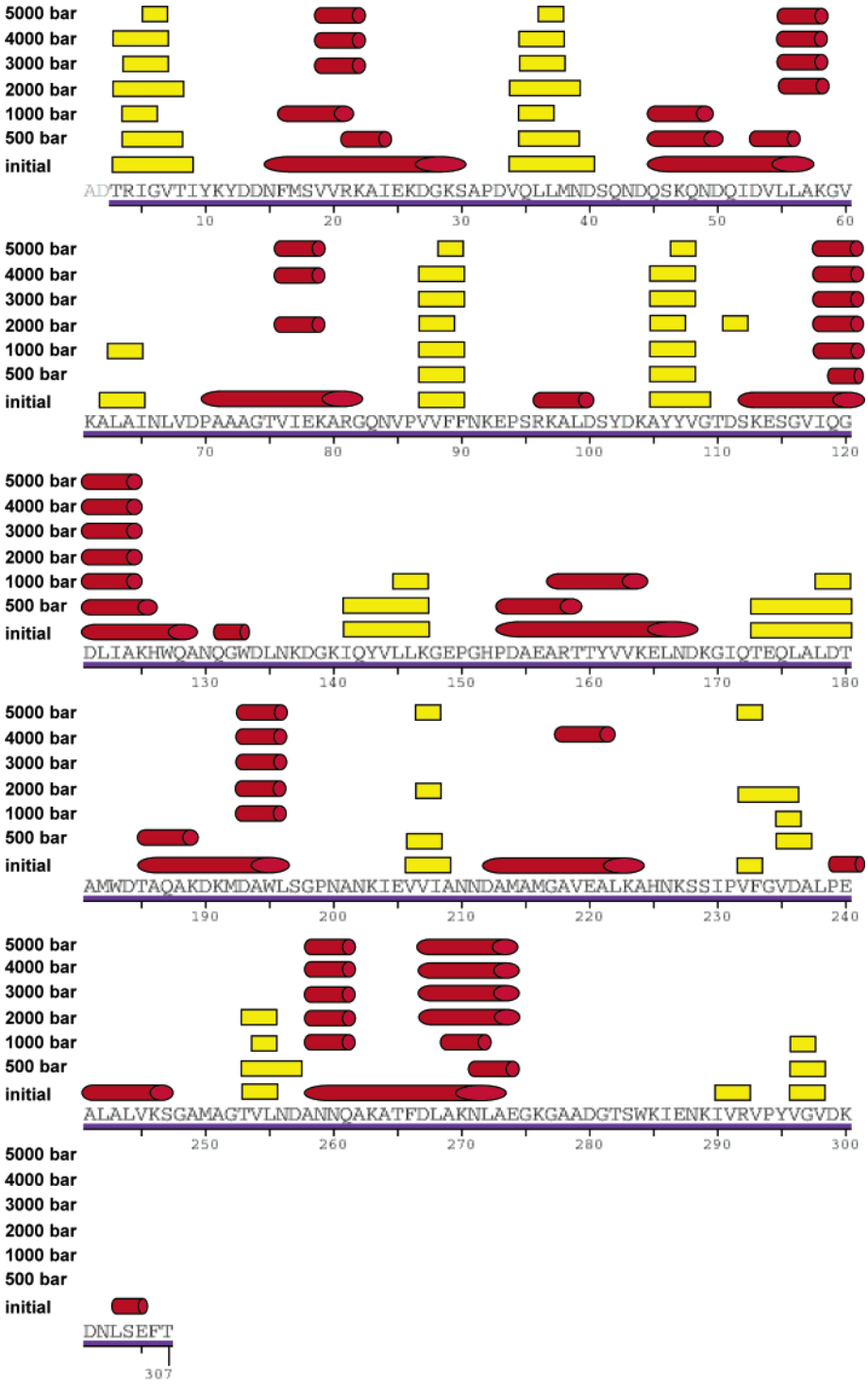

[a] α-Helices are represented as red cylinders and β-sheets as yellow rectangles. The sequence of GGBP from *S. typhimurium* is shown in one-letter code. The position of the secondary structures was identified by DSSP analysis.

larly compact structure. As it is shown in Figure 1, the presence of glucose does not affect remarkably the secondary structure of the protein since the band intensities in the 1700−1600 cm^{-1} interval are similar.

Pressure-Induced Denaturation and Changes in the Infrared Spectrum. Figure 2 shows the second-derivative and deconvolved spectra of GGBP and of GGBP/Glc as a function of the applied hydrostatic pressure. The increase in pressure leads to the decrease in intensity of the α-helix and β-sheet bands suggesting the pressure-induced loss of these secondary structural elements (protein denaturation). The decrease in intensity of the α-helix band is well visible in both deconvolved and second-derivative spectra of protein samples. In the GGBP spectrum recorded at 4172 bar (bold line) and in the GGBP/Glc spectrum recorded at 4969 bar (bold line) the α-helix band is slightly visible and not visible, respectively. At these pressures a band close to 1673 cm^{-1}, most likely due to turns, appears concomitantly with the

Scheme 2: Schematic Representation of the Changes in Secondary Structures (α-Helices and β-Sheets) of GGBP/Glc Subjected to Pressure Increases up to 5000 Bar[a]

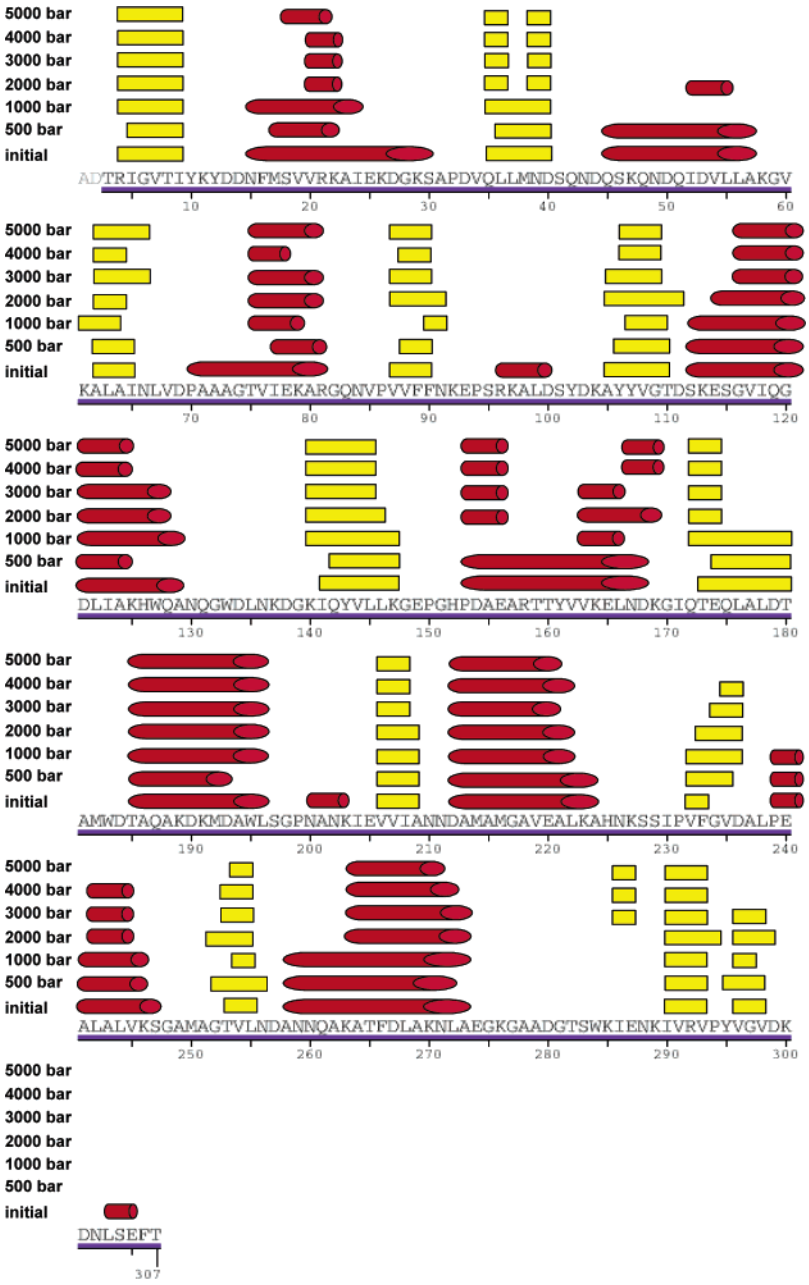

[a] α-Helices are represented as red cylinders and β-sheets as yellow rectangles. The sequence of GGBP from *S. typhimurium* is shown in one-letter code. The position of the secondary structures was identified by DSSP analysis.

disappearance of the band close to 1681 cm^{-1} (see second-derivative spectra). Indeed, this latter band decreases in intensity with the increase of pressure. Then, at higher pressures up to close 9000 bar, the shape of spectra does not change significantly. At the highest pressure the second-derivative and deconvolved spectra are characterized by a broad and asymmetrical band centered at about 1637 and 1639 cm^{-1}, respectively. Inspection of the spectra at wavenumbers higher than the band maximum (1637 or 1639 cm^{-1}) reveals, besides the well visible 1673 cm^{-1} band (turns), other small shoulders suggesting the presence of residual amide I′ components (α-helices) and unordered structures. Although occurring, the decrease in intensity of the β-sheet band with the increase in pressure is not as evident as in the case of the α-helix band (see also Figure 4). The spectra obtained at pressures close to 9000 bar are characterized by the bands close to 1637 or 1639 cm^{-1}, a position which is typical for the β-sheet structure. Hence, this result indicates that at high pressure the protein samples retain, in part, the β-sheets observed at atmospheric pressure. However, the broadness of the second-derivative and deconvolved spectra suggests that the 1637 or 1639 cm^{-1} bands are due also to absorption of unordered structures that typically absorb close to 1640 cm^{-1} (*26*).

The spectra in Figure 2 also show that the absorption at 1550 cm^{-1} (residual amide II band) decreases with the increase of pressure. In particular, the decrease of the above-mentioned band intensity is observed within the pressure interval from 1.0 to 5000 bar, while at higher pressures the band intensity remains almost stationary.

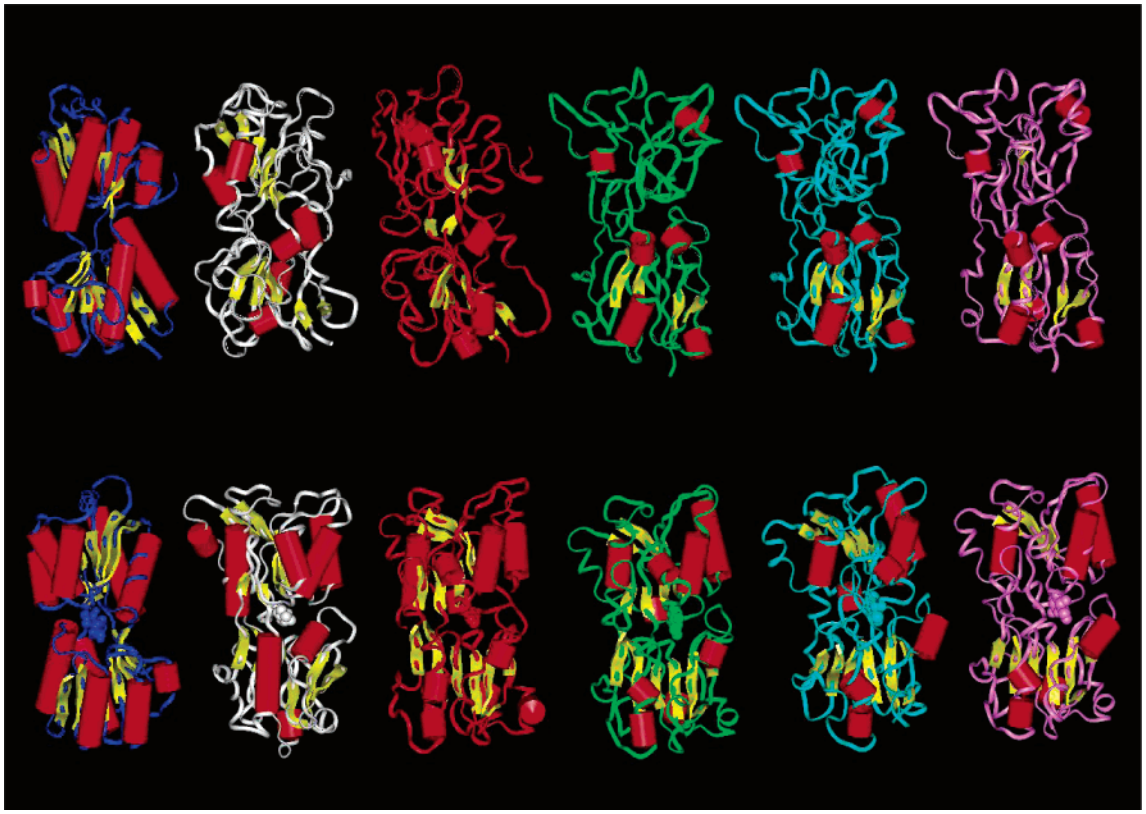

FIGURE 6: Comparison of the three-dimensional structures of GGBP (top) and GGBP/Glc (bottom) at increasing pressures. The first pictures on the left (blue backbone) were obtained by X-ray crystallography (files 1GCG.pdb on the top, 3GBP.pdb on the bottom). The other structures were obtained by averaging the conformations of GGBP and GGBP/Glc at pressure of 1000 bar (white backbone), 2000 bar (red backbone), 3000 bar (green backbone), 4000 bar (cyan backbone), and 5000 bar (pink backbone). Glucose in the GGBP/Glc complexes is represented in CPK mode. Secondary structure positions were identified by DSSP analysis. α-Helices are represented as red cylinders and β-sheets as yellow arrows. All structures are kept in the same relative orientation with the N-terminal domain in the upper part of the protein.

Protein denaturation may be followed by monitoring different parameters of the infrared spectrum (*33*, *34*). The width or position of the amide I′ band or the amide I′/amide II intensity ratio are affected by the applied pressure as shown in Figure 3. In all cases the midpoint transition ($P_{1/2}$) was higher in GGBP/Glc than in GGBP (see Table 1), indicating a protective effect of glucose against protein denaturation induced by high pressures. In particular, $P_{1/2}$ resulted at about 3800 and 4200 bar for GGBP and GGBP/Glc, respectively. Similar results were obtained by plotting the intensity of α-helix (1652 cm^{-1}) and β-sheet (1637 cm^{-1}) bands as a function of pressure (Figure 4, and Table 1). Hence, we can say that a remarkable loss of secondary structural elements occurs at about 3800 and 4200 bar for GGBP and GGBP/Glc, respectively, but residual secondary structures are still present in the samples at the highest pressure (Figure 2). Figure 3B shows the onset of drastic decrease in amide I′ band position at about 2900 bar for both GGBP and GGBP/Glc. In the 1−2900 bar range the amide I′ band position decreases linearly with the increase in pressure, the decrease being more marked in GGBP than in GGBP/Glc. This phenomenon is a general feature of proteins under pressure, and it is due to the elastic effect (*9*, *10*). Elastic effects are connected to changes in the length of chemical bonds, the hydration of a protein molecule, and reductions in size of molecular cavities (*9*). As pressure causes "compression" of chemical bonds, the decrease in amide I′ band position in proteins takes place as a consequence of the pressure-induced strengthening of the amide C═O···H hydrogen bond at the expense of the amide C═O bond (*10*). Elastic effects take place within relatively low range of pressure and they are always reversible and do not alter the molecular folding. On the other hand, at pressures higher than 2900 bar (Figure 3B), the decrease in amide I′ band position assumes a sigmoid-shaped function of pressure (*10*), phenomenon that is related to the plastic effect, i.e. unfolding and denaturation (*9*, *10*) as it is shown also by Figure 2A,C.

The decrease in intensity of the residual amide II band (Figure 2) may be ascribed to further $^1H/^2H$ exchange that may be caused by protein denaturation and/or to changes in the protein tertiary/quaternary structure (*33*, *34*). In the case of GGBP/Glc it should be mentioned that changes in the glucose binding equilibrium may alter the flexibility of the polypeptide chain allowing a deeper contact of the solvent (^2H_2O).

The pressure-dependent decrease in intensity of the residual amide II band (Figure 5A and Table 1) is very similar in GGBP and GGBP/Glc, the values of $P_{1/2}$ being equal to 3730 and 3805 bar, respectively. These pressure values are also similar to the $P_{1/2}$ values that reflect GGBP denaturation (Table 1). Hence, these data suggest that in GGBP the decrease in intensity of the residual amide II band is concomitant with protein denaturation. On the other hand, in GGBP/Glc the $P_{1/2}$ of protein denaturation is at about 4200 bar, while the $P_{1/2}$ for the decrease in intensity of the residual amide II band is about 3800 bar. This result suggests that

GGBP/Glc may undergo significant changes in tertiary structure followed by denaturation. A similar behavior has been already observed in studies of proteins under reducing conditions and exposed to high values of pressure (*19*).

Molecular Dynamics Simulations. Following our previous work (*12*), we pursued the analysis of the effect of high pressure on the conformation and dynamics of GGBP in the absence and in the presence of glucose. The protein used for MD simulations was that from *Salmonella typhimurium*, for which the structures of both unliganded and complexed proteins (*35*, *36*) are available in the PDB database (*37*). This protein shares about 95% sequence identity with GGBP from *E. coli*, and in particular the glucose-binding site is conserved between the two proteins. Using these two systems, it was possible to run the dynamic simulations for both systems exactly under the same conditions; while using the complex from *E. coli*, we would be forced to perturb the system with the deletion of glucose and a deep minimization prior the dynamics, thus altering the starting parameters. Furthermore, we were able to compare the results obtained in this work with those previously analyzed for the protein subjected to moderate pressure (*12*).

DSSP analysis on the average structures of GGBP and GGBP/Glc obtained after the MD simulations at high pressures, shown in Table 2, confirms the experimental findings that the effects of the pressure stress are different between the two systems. For example, the percentage of residues in random coil conformation rises up as the pressure increases, but this phenomenon is more pronounced in GGBP than in the GGBP/Glc complex. The DSSP analysis also reveals the increment of the presence of "noncanonical" secondary structures, like bend conformations or H-bonded turns, following the increase of external pressure. Also in this case, this effect is more pronounced in GGBP than in the GGBP/Glc complex. This confirms that the presence of the ligand in the binding cavity of GGBP is able to preserve more efficiently the global architecture of the protein and to contrast the loss of secondary structures in the presence of a pressure stress.

MD simulations also correlate well with experimental results in showing that α-helices appear to be less resistant than *β*-sheets to the pressure stress in both systems. In Schemes 1 and 2 we have summarized the variation in quantity and in position along the sequence of each secondary structure present in GGBP and GGBP/Glc, respectively, at increasing pressure values. It is possible to note that *β*-structures are generally preserved. On the contrary, α-helices appear to be disrupted or modified in length in both systems. The different sensitivity of these two secondary structures to the pressure stress is probably linked to the different resistance to mechanical deformation related to their shape and to the spatial distribution of the H-bonds that stabilize them.

Figure 6 shows the comparison of the tertiary structures of GGBP and GGBP/Glc at increasing pressure values. Looking at the different stages of protein perturbation induced by high pressure, we can deduce that the global structure of GGBP is markedly perturbed at pressure lower than 4000 bar. On the contrary, the structure of GGBP/Glc complex, even around 5000 bar, is sufficiently organized and preserved. In both systems the N-terminal domain retains more secondary structures than the C-terminal one. In particular, the central *β*-sheet in the N-terminal domain appears to be conserved in all proteins and in all conditions. On the contrary, the central *β*-sheet in the C-terminal domain in GGBP is disrupted at external pressure around 3000 bar, whereas in the GGBP/Glc complex it resists at higher pressures, although some strands that compose it are lost. Again, it is possible to note that α-helices composing the external part of the α/*β* barrel in both domains are the first structures to be perturbed by the increasing external pressure. In GGBP alone, at a pressure higher than 2000 bar they are present almost exclusively in the N-terminal domain, whereas in GGBP/Glc they are partially conserved also in the C-terminal domain.

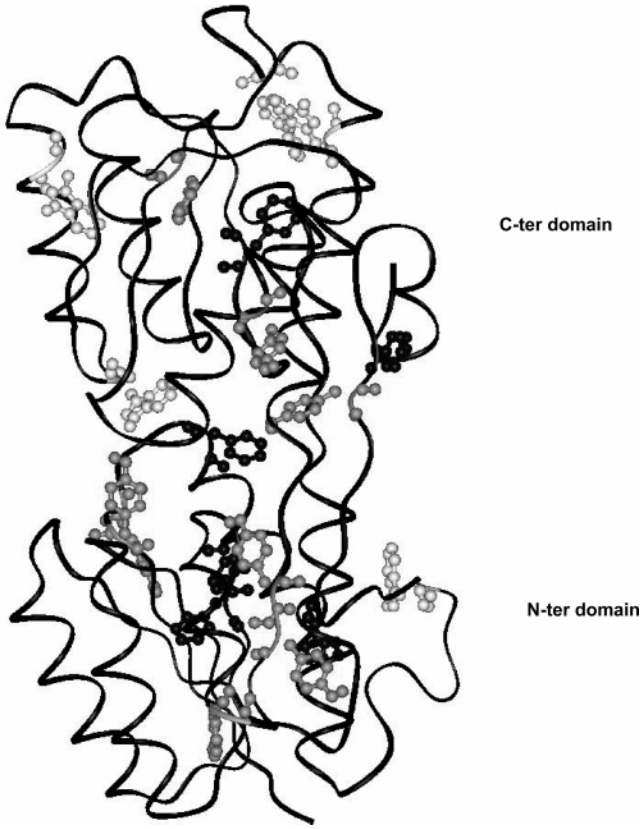

FIGURE 7: Aromatic amino acids in GGBP. The picture shows the structural distribution of Phe (dark gray), Tyr (light gray), and Trp (white) in the N-terminal and C-terminal domains of GGBP. The aromatic residues are represented in ball and stick mode.

The structure of biological macromolecules is stabilized mainly by three kinds of interactions, namely ionic, hydrophobic, and hydrogen bonding. Hydrostatic pressure affects these interactions in different ways. In particular, hydrophobic interactions are unfavorably affected at elevated pressure (*38*, *39*) and ionic interactions are weakened by high pressure due to electrostriction: each separated charge arranges water in its vicinity more densely than bulk water and thus the overall volume change favors the dissociation of ionic interaction under pressure (*38*). Since the formation of hydrogen bonds in biomacromolecules is connected to a negligibly small reaction volume which may be positive or negative, depending on the system (*38*), hydrogen bonds are less sensitive to pressure (*38*, *40*) than hydrophobic or ionic interactions. On the other hand, hydrophobic interactions between aromatics in the protein core are even reinforced by pressure (*40*). The importance of interactions between

Table 3: Percentage of Solvent Exposure of the Aromatic Amino Acids at Different Pressures, Calculated by NACCESS (All Atom Mode) for GGBP and GGBP/Glc[a]

	external pressure (bar)													
	initi al		500		1000		2000		3000		4000		5000	
system	GGBP	GGBP/Glc	GGBP	GGBP/Glc	GGBP	GGBP/Glc	GGBP	GGBP/Glc	GGBP	GGBP/Glc	GGBP	GGBP/Glc	GGBP	GGBP/Glc
N-Terminal Domain														
Tyr 10	3.6	2.8	4.4	1.2	4.4	13.2	19.0	8.5	12.8	3.0	5.4	0.6	9.3	2.9
Tyr 12	24.8	23.9	44.1	69.4	61.4	44.1	86.1	44.3	86.5	42.0	87.6	43.5	84.5	39.0
Phe 16	8.0	7.4	30.9	0	5.9	2.3	13.7	9.2	9.6	7.2	6.1	5.9	10.8	3.9
Phe 89	0.1	0.3	3.9	2.2	5.3	2.7	3.4	0.5	1.0	0.2	1.5	0.1	1.2	0.2
Phe 90	2.0	2.1	4.7	2.9	10.6	3.7	7.0	2.1	8.9	0.8	6.8	0.5	5.0	0.2
Tyr 102	6.7	4.9	6.1	36.6	11.9	41.1	20.6	87.8	19.7	100	20.7	100	23.0	100
Tyr 106	14.7	16.3	6.8	2.6	17.9	5.4	7.7	10.4	3.7	8.4	2.6	9.1	3.3	9.3
Tyr 107	2.1	2.3	1.4	0.2	0.8	0	2.3	0.5	2.8	0.3	2.0	0.2	2.5	0.4
Phe 266	5.0	6.1	28.2	5.4	10.6	20.3	15.3	21.0	12.8	21.4	6.3	15.8	8.3	18.8
Trp 284	21.4	19.8	59.2	23.2	47.1	17.5	48.5	16.8	61.3	17.3	63.0	17.2	69.4	17.2
C-Terminal Domain														
Trp 127	3.1	9.5	16.0	4.9	3.0	0.5	2.0	0.9	1.7	0.5	0.5	0.4	1.7	0.4
Trp 133	16.4	18.3	2.9	15.6	37.2	8.1	38.3	5.0	37.8	4.7	35.2	3.1	33.8	2.8
Tyr 143	3.2	3.2	13.9	8.4	5.9	8.7	26.4	17.5	24.2	11.3	21.3	10.9	23.1	11.2
Tyr 161	33.8	27.7	61.4	35.7	26.6	48.8	44.9	74.9	51.1	78.4	61.5	79.6	53.1	66.1
Trp 183	10.4	9.7	26.1	0.7	15.5	1.1	38.8	8.7	31.7	7.5	27.0	8.2	36.6	8.5
Trp 195	13.0	13.5	47.4	17.6	13.0	6.8	27.3	37.4	27.2	27.9	21.7	23.9	25.9	24.8
Phe 233	0	0	0.1	0.6	1.7	0.3	0	2.6	0	2.5	0	0.4	0	0.2
Tyr 295	4.4	4.0	12.7	3.1	5.1	7.1	9.4	6.8	8.9	0.9	4.9	0.4	9.4	0
Phe 306	31.4	26.3	61.3	32.5	61.0	97.8	71.5	50.5	60.7	44.2	61.9	37.1	59.0	34.9

[a] The results were calculated on the crystallographic structures at the initial stage and on the average structures for the other pressures. Data at 500, 1000, and 2000 bar refer to the structures presented in Marabotti et al. (*9*) and are reported here to aid the comparison.

aromatic side chains for the protein piezostability was demonstrated in Sso7d, a DNA-binding protein from *Sulfolobus solfataricus* (*41*). Sso7d is rich in β-sheets and has an aromatic cluster consisting of several interacting residues, and Phe31 is located in the core of the cluster itself. The single mutation F31A abolished the interactions of F31 with the other aromatics and caused a dramatic loss in piezostability of the protein (*41*, *42*).

In an attempt to explain the higher resistance of the N-terminal than the C-terminal domain toward high pressures we inspected the structure of GGBP and the amino acid composition of the two domains. We found that in the N-terminal domain are present four Phe (Phe 16, 89, 90, 266), five Tyr (Tyr 10, 12, 102, 106, 107), and one Trp (Trp 284), while in the C-terminal domain are present two Phe (Phe 233, 306), three Tyr (Tyr 143, 161, 295), and four Trp (Trp 127, 133, 183, 195). Despite the similar quantity of aromatic residues in the two domains, in the N-terminal domain of GGBP several residues (namely Phe 89, Phe 90, Tyr 102, Tyr 106, Tyr 107, and Trp 284) are clustered together in the core of the domain itself. On the contrary, the aromatic amino acids in the C-terminal domain are not forming clusters, but are "spread" in several parts of the domain architecture (Figure 7). The same is true for GGBP/Glc (data not shown). Moreover, an analysis performed by NACCESS on the solvent exposure of aromatic amino acid (Table 3) shows that, at atmospheric pressure, 7 out of 10 residues in the N-terminal domain of GGBP and GGBP/Glc are buried (less than 10% of the relative solvent accessibility), whereas 5 out of 9 aromatic residues in GGBP and 4 out of 9 in GGBP/Glc are exposed to the solvent in the C-terminal domain. Looking at the changes in exposure during the application of high external pressures, it is possible to note that in general a higher exposure to the solvent of these side chains is evident for both systems, suggesting a general weakening of hydrophobic interactions between bulky side chains, in agreement with previous reports (*38*, *39*, *41*, *42*). Nevertheless, for GGBP the exposure of aromatic residues is always lower in the N-terminal domain with respect to the C-terminal domain, whereas it is more or less the same in GGBP/Glc. This observation parallels the above-reported data that the central β-sheet of the C-terminal domain is completely lost at high pressure in GGBP, but partially conserved in GGBP/Glc.

These findings and the fact that interactions of aromatic side chains are important for the stability of the protein at high pressure suggest that the higher piezostability of the N-terminal than the C-terminal of GGBP is probably due to a higher number of aromatic side chains in the former domain that may undergo interactions.

CONCLUSIONS

FT-IR spectroscopy together with MD simulations allowed us to obtain a detailed portrait of the effect of pressure on the protein structure. In fact, the simulation experiments were performed to predict how the pressure impacts on each single structural element of the protein, thus suggesting a precise molecular interpretation of the single events, leading to global conformational changes that are experimentally detectable by means of the spectroscopic measurements.

ACKNOWLEDGMENT

The authors thank Dr. Susan Costantini, Laboratory of Bioinformatics, ISA, Avellino, for providing a tool for the calculation of the percentage of secondary structures from a DSSP file.

REFERENCES

1. Dumay, E., Picart, L., Regnault, S., and Thiebaud, M. (2006) High pressure-low temperature processing of food proteins, *Biochim. Biophys. Acta 1764*, 599−918.
2. Hayashi, R. (2002) High pressure in bioscience and biotechnology: pure science encompassed in pursuit of value, *Biochim. Biophys. Acta 1595*, 397−399.

3. Ernst, R. R. (2002) Preface, *Biochim. Biophys. Acta 1595*, 1−2.
4. Meersman, F., and Dobson, C. M. (2006) Probing the pressure−temperature stability of amyloid fibrils provides new insights into their molecular properties, *Biochim. Biophys. Acta 1764*, 452−460.
5. Ribó, M., Font, J., Benito, A., Torrent, J., Lange, R., and Vilanova, M. (2006) Pressure as a tool to study protein-unfolding/refolding processes: The case of ribonuclease A, *Biochim. Biophys. Acta 1764*, 461−469.
6. Weber, G., and Drickamer, H. G. (1983) The effect of high pressure upon proteins and other biomolecules, *Q. Rev. Biophys. 16*, 89−112.
7. Staiano, M., Bazzicalupo, P., Rossi, M., and D'Auria, S. (2005) Glucose biosensors as models for the development of advanced protein-based biosensors, *Mol. BioSystem. 1*, 5/6 354−362.
8. Ross, A. I., Griffiths, M. W., Mittal, G. S., and Deeth, H. C. (2003) Combining non-thermal technologies to control foodborne microorganisms, *Int. J. Food Microbiol. 89*, 125−138.
9. Heremans, K., and Smeller, L. (1998) Protein structure and dynamics at high pressure, *Biochim. Biophys. Acta 1386*, 353−370.
10. Dzwolak, W., Kato, M., and Taniguchi, Y. (2002) Fourier transform infrared spectroscopy in high-pressure studies on proteins, *Biochim. Biophys. Acta 1595*, 131−144.
11. Paci, E. (2002) High pressure simulations of biomolecules, *Biochim. Biophys. Acta 1595*, 185−200.
12. Marabotti, A., Herman, P., Staiano, M., Varriale, A., de Champdoré, M., Rossi, M., Gryczynski, Z., and D'Auria, S. (2006) Pressure effect on the stability and the conformational dynamics of the D-galactose/D-glucose-binding protein from *Escherichia coli*, *Proteins 62*, 193−201.
13. Vyas, N. K., Vyas, M. N., and Quiocho, F. A. (1988) Sugar and signal transducer binding sites of *Escherichia coli* galactose chemoreceptor protein, *Science 242*, 1290−1295.
14. Tolosa, L., Gryczynski, I., Eichhorn, L. R., Dattelbaum, J. D., Castellano, F. N., Rao, G., and Lakowicz, J. R. (1999) Glucose sensor for low-cost lifetime-based sensing using a genetically engineered protein, *Anal. Biochem. 267*, 114−120.
15. Bradford, M. M. (1976) A rapid and sensitive method for the quantitation of microgram quantities of protein utilizing the principle of protein-dye binding, *Anal. Biochem. 72*, 248−254.
16. Tanfani, F., Lapathitis, G., Bertoli, E., and Kotyk, A. (1998) Structure of yeast plasma membrane H^+-ATPase: comparison of activated and basal-level enzyme forms, *Biochim. Biophys. Acta 1369*, 109−118.
17. Salomaa, P., Schaleger, L. L., and Long, F. A. (1964) Solvent deuterium isotope effects on acide-base equilibria, *J. Am. Chem. Soc. 86*, 1−7.
18. Wong, P. T. T., and Moffat, D. J. (1989) A new internal pressure calibrant for high-pressure infrared spectroscopy of aqueous systems, *Appl. Spectrosc. 43*, 1279−1281.
19. Meersman, F., and Heremans, K. (2003) High pressure induces the formation of aggregation-prone states of proteins under reducing conditions, *Biophys. Chem. 104*, 297−304.
20. Meersman, F., Smeller, L., and Heremans, K. (2002) Comparative Fourier transform infrared spectroscopy study of cold-, pressure-, and heat-induced unfolding and aggregation of myoglobin, *Biophys. J. 82*, 2635−2644.
21. Kabsch, W., and Sander, C. (1983) Dictionary of protein secondary structure: pattern recognition of hydrogen-bonded and geometrical features, *Biopolymers 22*, 2577−2637.
22. Hubbard, S. J., Campbell, S. F., and Thornton, J. M. (1991) Molecular recognition. Conformational analysis of limited proteolytic sites and serine proteinase protein inhibitors, *J. Mol. Biol. 220*, 507−530.
23. D'Auria, S., Alfieri, F., Staiano, M., Pelella, F., Rossi, M., Scirè, A., Tanfani, F., Bertoli, E., Grycznyski, Z., and Lakowicz, J. R. (2004) Structural and thermal stability characterization of *Escherichia coli* D-galactose/D-glucose-binding protein, *Biotechnol. Prog. 20*, 330−337.
24. D'Auria, S., Ausili, A., Marabotti, A., Varriale, A., Scognamiglio, V., Staiano, M., Bertoli, E., Rossi, M., and Tanfani, F. (2006) Binding of glucose to the D-galactose/D-glucose-binding protein from *Escherichia coli* restores the native protein secondary structure and the thermostability that are lost upon calcium depletion. *J. Biochem. 139*, 213−221.
25. Herman, P., Vecer, J., Bervik, I., Jr., Staiano. M., de Champdoré, M., Varriale, A., Rossi, M., and D'Auria, S. (2005) The role of calcium in the conformational dynamics and thermal stability of the D-galactose/D-glucose-binding protein from *E. coli*, *Proteins 61*, 184−195.
26. Arrondo, J. L., Muga, A., Castresana, J., and Goñi, F. M. (1993) Quantitative studies of the structure of proteins in solution by Fourier transform infrared spectroscopy, *Prog. Biophys. Mol. Biol. 59*, 23−56.
27. Surewicz, W. K., Mantsch, H. H., and Chapman, D. (1993) Determination of protein secondary structure by Fourier transform infrared spectroscopy: A critical assessment, *Biochemistry 32*, 389−394.
28. Krimm, S., and Bandekar, J. (1986) Vibrational spectroscopy and conformation of peptides, polypeptides and proteins, *Adv. Protein Chem. 38*, 181−364.
29. Chirgadze, Y. N., Fedorov, O. V., and Trushina, N. P. (1975) Estimation of amino acid residue side-chain absorption in the infrared spectra of protein solutions in heavy water, *Biopolymers 14*, 679−694.
30. Barth, A. (2000) The infrared absorption of amino acid side chains, *Prog. Biophys. Mol. Biol. 74*, 141−173.
31. Barth, A., and Zscherp, C. (2002) What vibrations tell us about proteins, *Q. Rev. Biophys. 35*, 369−430.
32. Osborne, H. B., and Nabedryk-Viala, E. (1982) Infrared measurements of peptide hydrogen exchange in rhodopsin, *Methods Enzymol. 88*, 676−680.
33. D'Auria, S., Herman, P., Lakowicz, J. R., Tanfani, F., Bertoli, E., Manco, G., and Rossi, M. (2000) The esterase from the thermophilic eubacterium *Bacillus acidocaldarius*: structural-functional relationship and comparison with the esterase from the hyperthermophilic archaeon *Archaeoglubus fulgidus*, *Proteins 40*, 473−481.
34. Pedone, E., Bartolucci, S., Rossi, M., Pierfederici, F. M., Scirè, A., Cacciamani, T., and Tanfani, F. (2003) Structural and thermal stability analysis of *Escherichia coli* and *Alicyclobacillus acidocaldarius* thioredoxin revealed a molten globule-like state in the thermal denaturation pathway of the proteins: an infrared spectroscopic study, *Biochem. J. 373*, 875−883.
35. Flocco, M. M., and Mowbray, S. L. (1994) The 1.9 Å X-ray structure of a closed unliganded form of the periplasmic glucose/galactose receptor from *Salmonella typhimurium*, *J. Biol. Chem. 269*, 8931−8936.
36. Mowbray, S. L., Smith, R. D., and Cole, L. B. (1990) Structure of the periplasmic glucose/galactose receptor of *Salmonella typhimurium*, *Receptor 1*, 41−53.
37. Berman, H., Henrick, K., and Nakamura, H. (2003) Announcing the worldwide Protein Data Bank, *Nat. Struct. Biol. 10*, 980.
38. Gross, M., and Jaenicke, R. (1994) Proteins under pressure. The influence of high hydrostatic pressure on structure, function and assembly of proteins and protein complexes, *Eur. J. Biochem. 221*, 617−630.
39. Marchal, S., Torrent, J., Masson, P., Kornblatt, J. M., Tortora, P., Fusi, P., Lange, R., and Balny, C. (2005) The powerful high pressure tool for protein conformational studies, *Braz. J. Med. Biol. Res. 38*, 1175−1183.
40. Mombelli, E., Shehi, E., Fusi, P., and Tortora, P. (2002) Exploring hyperthermophilic proteins under pressure: theoretical aspects and experimental findings, *Biochim. Biophys. Acta 1595*, 392−396.
41. Mombelli, E., Afshar, M., Fusi, P., Mariani, M., Tortora, P., Connelly, J. P., and Lange, R. (1997) The role of phenylalanine 31 in maintaining the conformational stability of ribonuclease P2 from *Sulfolobus solfataricus* under extreme conditions of temperature and pressure, *Biochemistry 36*, 8733−8742.
42. Fusi, P., Goossens, K., Consonni, R., Grisa, M., Puricelli, P., Vecchio, G., Vanoni, M., Zetta, L., Heremans, K., and Tortora, P. (1997) Extreme heat- and pressure-resistant 7-kDa protein P2 from the archaeon *Sulfolobus solfataricus* is dramatically destabilized by a single-point amino acid substitution, *Proteins 29*, 381−390.

BI061158K